SOL-GEL COATINGS ON ACOUSTIC WAVE DEVICES: THIN FILM CHARACTERIZATION AND CHEMICAL SENSOR DEVELOPMENT

GREGORY C. FRYE, C. JEFFREY BRINKER, ANTONIO J. RICCO, STEPHEN J. MARTIN, JANICE HILLIARD, AND DANIEL H. DOUGHTY
Sandia National Laboratories, Albuquerque, NM 87185

SAND--89-2802C

DE90 012224

ABSTRACT

We have investigated the use of porous oxide coatings, formed using sol-gel chemistry routes, as the discriminating elements of acoustic wave (AW) chemical sensors. These coatings provide several unique advantages: durability, high adsorption capacity based on large surface areas, and chemical selectivity based on both molecular size and chemical interactions. The porosity of these coatings is determined by performing nitrogen adsorption isotherms using the AW device response to mass changes to monitor the uptake of nitrogen at 77 K. These studies demonstrate how sol-gel chemistry and film-forming technique can be used to tailor the microstructure of thin oxide coatings. The chemical sensitivity and selectivity obtained with this class of coatings will be demonstrated using several examples: hydrous titanate ion exchange coatings, zeolite/silicate microcomposite coatings, and surface-modified silicate films.

INTRODUCTION

Sol-gel chemistry involves the hydrolysis and condensation of metal alkoxides to form inorganic polymers in solution [1]. By varying the reaction conditions (e.g., reaction protocol, concentration of catalyst, water or alkoxide), the structure of these polymers can be varied from weakly branched chains to highly ramified structures (i.e., resembling a tumbleweed) to dense colloidal particles [2]. Prior to gelation, films can be prepared from these solutions by either spin- or dip-coating. The final film structure is dictated by the film forming procedure and the polymer structure: dense films are formed from weakly branched polymers, while high surface area porous films are formed from highly ramified polymers or dense colloidal particles [3]. The pore size distribution in the porous films can be tailored by varying the size and shape of the precursor polymers as well as by varying the coating procedure or thermal treatment [4].

In this paper, the application of these controlled microstructure oxide coatings for chemical sensor coatings will be discussed. Coatings that provide both chemical selectivity and increased sensitivity are critical for the development of effective chemical sensors [5,6]. Chemical selectivity can be obtained based on selective sorption of a single species or a class of species. Increased sensitivity can be obtained based on high sorption capacities. Some examples of the types of sensor coatings that have been employed are organic polymers [5,7], phthalocyanines [5] and biological agents [8]. For sensors based on AW devices, gas phase sensors utilizing surface acoustic wave devices [5,7] and liquid phase sensors utilizing either acoustic plate mode devices [9] or Lamb wave devices [8] have been developed.

Porous oxide coatings can provide several unique advantages as the discriminating elements of chemical sensors: (1) resistance to thermal or chemical degradation, (2) high surface area and pore volume resulting in increased sensitivity based on large sorption capacities, (3) controlled microstructure (i.e., pore size distribution) providing chemical discrimination based on molecular size, (4) capability to easily modify the chemical nature of the surfaces to provide discrimination based on chemical interactions, and (5) minimal changes in film properties (e.g., viscoelastic properties) during sorption resulting in simplified

---

analysis of sensor response. Specific examples to be discussed are: (1) the use of SAW devices coated with zeolite microcrystals embedded in a dense sol-gel matrix to provide chemical selectivity based on molecular size, (2) the use of APM devices coated with hydrous oxides with large ion exchange capacities for sensing ionic species in solution, and (3) the addition of chemically reactive surface groups to porous oxide films using silane coupling agents.

Acoustic Wave Devices

Acoustic wave devices consist of input and output interdigital transducers formed on a piezoelectric substrate such as quartz or lithium niobate. When an alternating voltage is applied to the input transducer, it generates an alternating mechanical strain field (due to the piezoelectric nature of the substrate). This launches an acoustic wave which travels along the surface (e.g., a surface acoustic wave: SAW) or through the bulk of the substrate (e.g., an acoustic plate mode: APM). This wave will interact with a thin film formed on the device surface before being converted back into an electrical signal by the output transducer. This interaction results in an alteration of the velocity of the wave.

Changes in wave velocity can easily be determined by operating the device as the feedback element of an oscillator circuit using an RF amplifier. In this configuration, changes in frequency (f) can be directly related to changes in wave velocity (v). In situations where the velocity shift (Δv) is dominated by changes in the mass density of the film, these frequency changes (Δf) can be directly related to changes in mass density Δm (mass/area) using:

$$\frac{\Delta f}{f_o} = \frac{\Delta v}{v_o} = - c_m \Delta m , \qquad (1)$$

where v_o and f_o represent the unperturbed velocity and frequency, respectively. The parameter c_m is a mass sensitivity constant which depends on the piezoelectric substrate, the acoustic wave being used, and the device frequency. To illustrate the extreme sensitivity of these devices, the 97 MHz SAW devices used in this study have a typical short term frequency stability in operation on the order of 10 Hz, giving a mass resolution of 0.8 ng/cm^2 of film (c_m = 125 cm^2/g for this device).

Surface acoustic waves resemble a wave on water, exhibiting displacement in the direction of propagation as well as normal to the substrate. If a liquid is placed in contact with a SAW device, the normal component of displacement results in the generation of compressional waves in the liquid. These compressional waves carry the acoustic power away from the substrate making the SAW device inoperable. However, acoustic plate modes having displacement in the plane of the substrate and perpendicular to the direction of propagation can also be excited [9]. When a liquid is placed in contact with an APM device, only viscous coupling of the wave occurs. This results in a relatively small amount of wave attenuation, making these devices effective as liquid phase sensors. In addition, these waves travel through the bulk of the crystal with equal amplitude at both surfaces. This allows the liquid to be contacted to the unelectroded side of the crystal, protecting the transducers from the liquid. APM devices can also act as extremely sensitive microbalances. For the 158 MHz APM device used in this study, the mass sensitivity is within a factor of three of the SAW device (c_m = 43 cm^2/g, determined by monitoring frequency during the vacuum evaporation of metal onto the substrate). Additional details on both SAW [5] and APM [9] devices are given elsewhere.

RESULTS AND DISCUSSION

Characterization of Film Porosity

In developing oxide coatings for chemical sensors, the microstructural properties of potential films have been characterized. The frequency response of a coated SAW device is used to monitor the uptake of nitrogen (at 77 K) as a function of the partial pressure (p) of nitrogen in the gas phase over the device. This type of measurement, called a nitrogen adsorption isotherm, can be used to determine [10]: (1) sample surface area using the BET analysis, (2) total pore volume based on the maximum uptake at partial pressures close to the saturation vapor pressure (p_o) at the temperature of the run, and (3) pore size distributions based on an analysis considering capillary condensation into the pores.

The experimental system used for these measurements is shown in Fig. 1. To remove adsorbed species from the surfaces of the film prior to a run, the test case and a coil on the gas inlet side are placed in an oven and heated to 160 °C for two hours under dry nitrogen. A pure helium stream is then passed over the device while the test case and coil are immersed in a dewar flask of liquid nitrogen to maintain the device and gas stream at 77 K. During a run, computer-operated mass flow controllers are used to vary the relative flow rates of a nitrogen carrier stream and a nonadsorbing helium mix-down stream. In this way, normalized nitrogen partial pressure (p/p_o) is varied from zero to about 0.95 and back to zero. Nitrogen adsorption isotherms obtained in this manner for two films are shown in Fig. 2. The sol-gel system used contains SiO_2, B_2O_3, Al_2O_3 and BaO in ratios (by weight) of 71:18:7:4 (details of the sol-gel preparation are presented elsewhere [11]). Films were formed on the SAW device surface by dip-coating followed by a 400 °C anneal for 5 minutes.

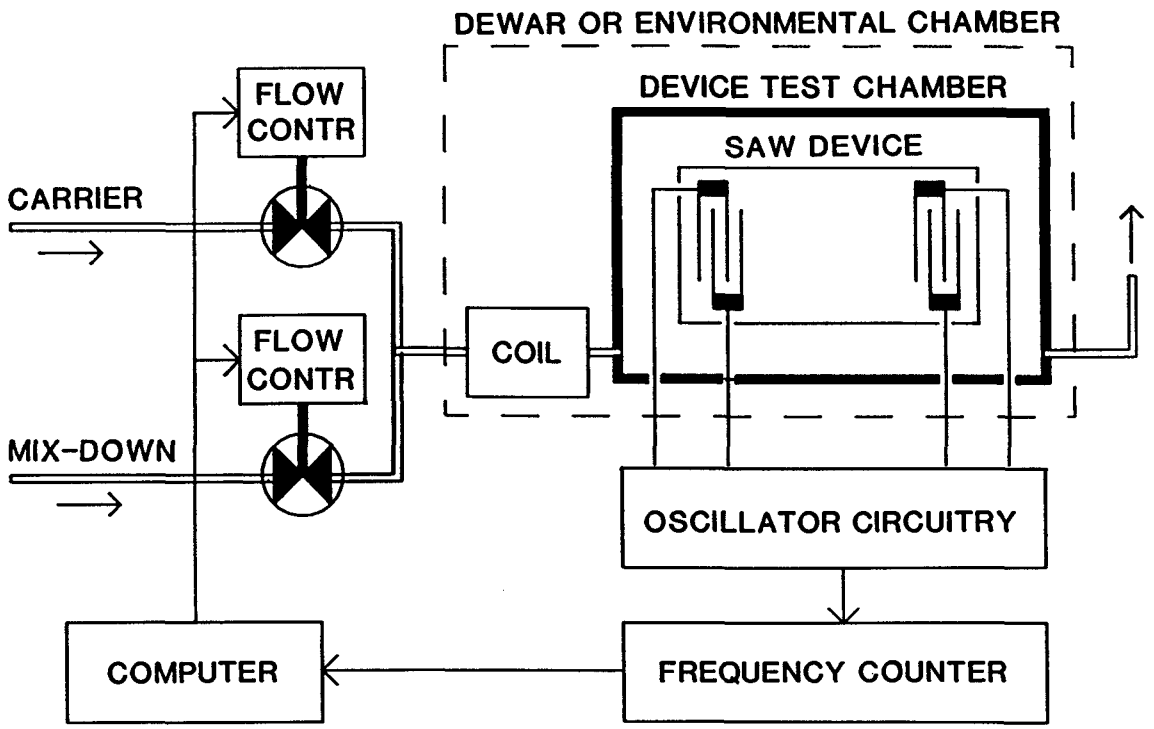

Fig. 1: Schematic of experimental system used to monitor nitrogen adsorption on the surfaces of porous thin films formed on SAW devices. The device is maintained at 77 K by immersion in a dewar flask filled with liquid N_2. The N_2 partial pressure is controlled by varying the relative flow rates of N_2 and He streams while the mass of adsorbed N_2 is determined by monitoring changes in the SAW frequency.

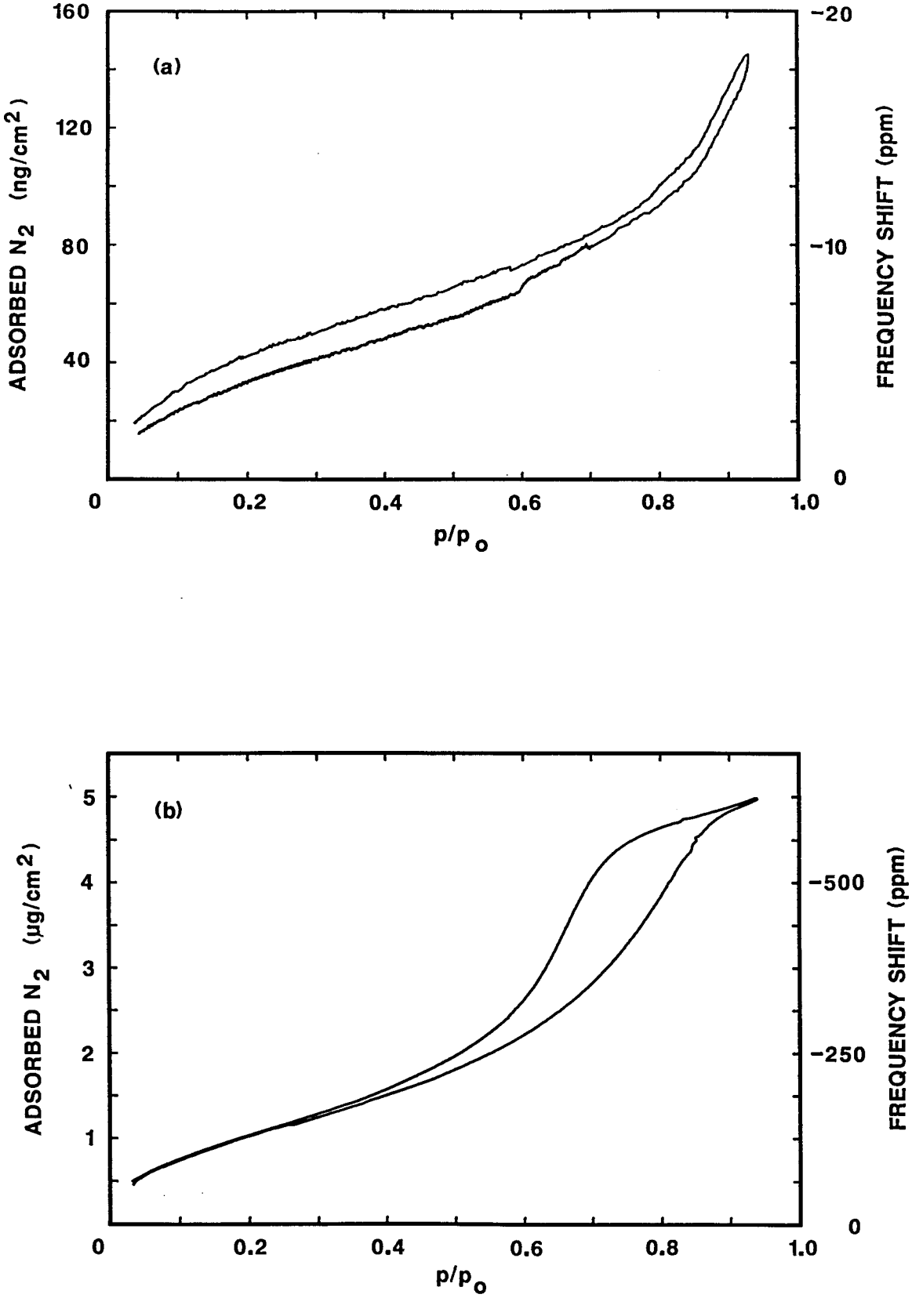

Fig. 2: Nitrogen adsorption isotherms using coated SAW devices for films formed from (a) unaged and (b) aged sol-gel solutions. A BET surface area of 1.3 cm^2/cm^2 of film for the unaged indicates this film is nonporous while a value of 33 cm^2/cm^2 obtained for the aged film indicates it is highly porous.

The first film (Fig. 2a) was formed by dip-coating using the initially prepared sol-gel solution which contains very small polymer precursors (hydrodynamic radius ~3 nm). The total amount of adsorption is small and the shape of the isotherm is Type II, typical of nonporous samples [10]. The BET surface area is 1.3 cm^2/cm^2 of film, very close to the value of 1.0 cm^2/cm^2 expected for a flat, nonporous film (the slightly higher value may be indicative of surface roughness). These results agree with ellipsometric (Rudolph AutoEL IV) analysis which gives a film thickness of 120 nm and a refractive index of 1.46, very close to the value expected for a dense film of this composition.

The second film (Fig. 2b) was formed by dip-coating after aging the same solution for three weeks at 50 °C and pH 3. This aging results in larger (hydrodynamic radius ~25 nm), highly ramified polymeric species which, due to their inability to interpenetrate, create porosity in the film [3]. This porosity is verified by ellipsometry which gives a refractive index of 1.18, indicating a volume percent porosity of 56%. This agrees with a value of 52% calculated based on the amount of adsorption at the high partial pressure end of the isotherm and a film thickness from ellipsometry of 148 nm. The isotherm shape is Type IV, typical of porous samples with pore diameters in the range of 3 to 50 nm. The BET surface area is 33 cm^2/cm^2, indicating a significant amount of porosity for this thin film (this value implies a surface area of ~250 m^2/g of film). Using multiple coats to obtain a film thickness on the order of 1 μm, surface area enhancements of 200 or more could be obtained with this system.

The pore size distribution obtained from the desorption branch of the isotherm for the porous film (Fig. 2a) is shown in Fig. 3. A unimodal distribution with a median pore diameter of 6.2 nm is obtained. Even though these pores are too large to exclude many species on the basis of size, smaller pore sizes are obtained with this system using shorter aging times [4,11]. This allows the pore size to be varied over a significant range by simply varying the aging time prior to film formation. Additional details on the characterization of this system as well as on the use of different reaction protocols (e.g., acid vs. base catalysis) are presented elsewhere [4,11,12].

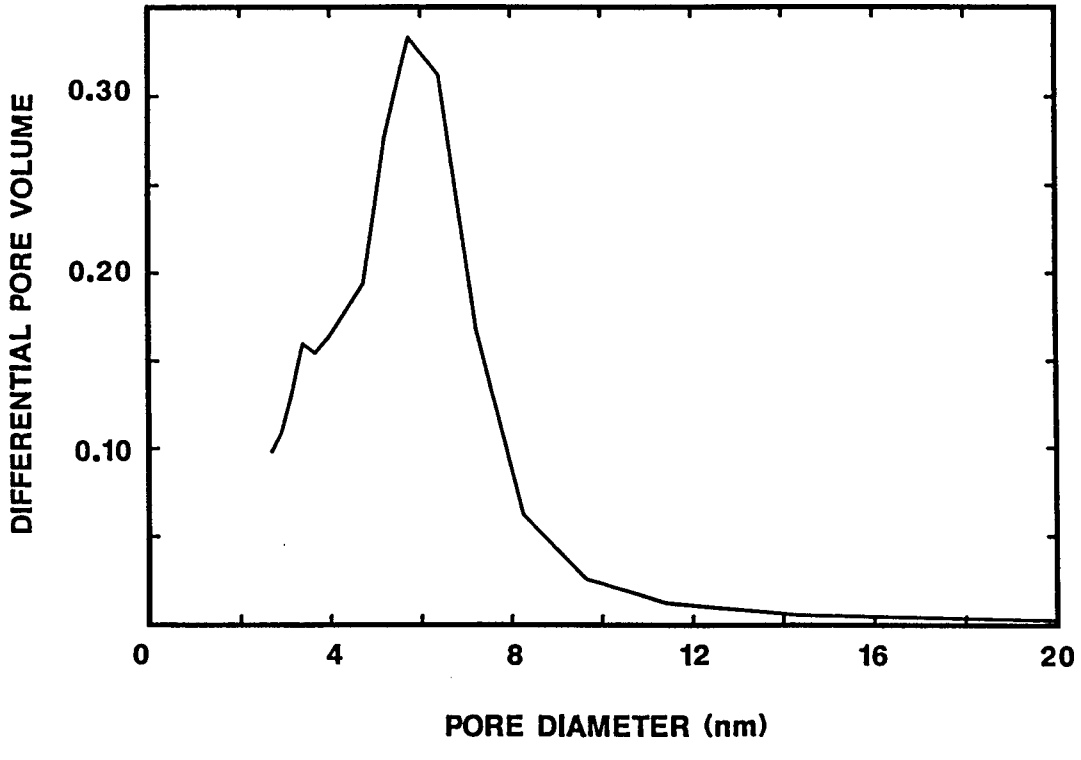

Fig. 3: Pore size distribution obtained from the desorption branch of the nitrogen adsorption isotherm for the film formed from the aged sol-gel solution (see Fig. 2b). A median pore diameter of 6.2 nm is obtained.

To investigate the effect of film-forming procedure on film microstructure, two SAW devices were dip-coated from the same sol-gel solution followed by a 400 °C anneal for 10 minutes. The solution, prepared according to the Stöber process [13], resulted in colloidal silicate particles having a diameter of 55 nm. The only difference between the two coatings was the dip-coating rate: 5 versus 18 inch/min. The results of the SAW nitrogen adsorption studies are listed in Table I. Theoretical values for the surface area and percent porosity are also listed. These values were calculated based on the refractive index and film thickness (obtained using ellipsometry) and the known particle size. The faster dip coating rate entrains a thicker layer of the solution which results in a significantly thicker film (130 and 260 nm for 5 and 18 inch/min, respectively). This thicker coating results in a higher surface area. The BET surface areas obtained from the SAW nitrogen adsorption isotherms are in good agreement with the calculated values, helping to verify the absolute accuracy of this technique.

The faster coating rate also appears to result in a denser particle packing. This is reflected in lower values for percent porosity for the 18 inch/min sample. Percent porosity was calculated from the nitrogen adsorption isotherms by determining the volume of nitrogen adsorbed (per unit area) at high partial pressures ($p/p_o = 0.96$) and comparing to the film thicknesses. Percent porosity from the refractive index was calculated using the Lorentz-Lorenz relationship and a skeletal refractive index of 1.4 (calculated for 90% density in the matrix and a refractive index of 1.45 for a fully dense material at this composition). The refractive index values were 1.228 and 1.262 for the 5 and 18 inch/min samples, respectively. The experimental SAW values and the calculated values are again in good agreement for both films tested. The denser packing at the faster rate is also seen in smaller values for the median pore diameter (calculated from the desorption branch). The results of these studies are useful in determining how to tailor surface area and pore size to fit a given sensing application based on controlling sol-gel chemistry, reaction protocols or film-forming technique.

Table I: Comparison of experimental (SAW nitrogen adsorption) and calculated values for the properties of films formed at two dip-coating rates from solutions of 55 nm diameter silicate particles formed by the Stöber process [13].

Dip Coating Rate (inch/min)	Percent Porosity		Surface Area (cm^2/cm^2 of film)		Median Pore Diameter (nm)
	Nitrogen Adsorption ($p/p_o = 0.96$)	Calculated (Refractive Index)	Nitrogen BET	Calculated	
5	36%	40%	8.7	8.6	18.1
18	27%	32%	16.4	19.9	15.0

Zeolite/Silicate Microcomposite Coatings

The most dramatic demonstration of chemical selectivity based on size exclusion will be obtained with a film with a single characteristic pore size. Sol-gel chemical routes can provide a narrow range of pore sizes; however, the random nature of this process always results in a distribution in pore sizes (see Fig. 3). One model inorganic porous system with unimodal pore sizes is the zeolites (molecular sieves). The most common zeolites are aluminosilicates which, due to their cagelike crystalline structures, have a single pore size that dictates accessibility to molecular adsorbate species. For example, the ZSM-5 zeolite has an opening with dimensions of 0.55 by 0.60 nm.

Zeolites can be synthesized using hydrothermal techniques. By rapid quenching at the early stages of the reaction, small (< 1 μm crystallite size) ZSM-5 crystals are formed [14]. To create an AW device coating that utilizes the unimodal pore size of zeolites, these small crystals are embedded in a dense thin-film sol-gel matrix [15]. This matrix forces adsorption to occur exclusively within the zeolite channel system. SEM analysis shows that the zeolites protrude from the sol-gel matrix. Quantitative titration of intrazeolite acid sites with organic bases such as pyridine indicate that the zeolite channels remain accessible [16].

The selectivity of a SAW device coated with this ZSM-5 zeolite/silicate microcomposite film has been previously demonstrated using molecular probes with kinetic diameters ranging from 0.38 to 0.62 nm [16]. At relatively low vapor concentrations (0.1% of saturation for each species), large frequency shifts were observed for methanol and isopropanol, which have kinetic diameters (0.38 and 0.47 nm, respectively) less than the zeolite pore size. These frequency shifts indicate significant amounts of adsorption in the pores of the zeolite crystals: 540 and 840 ng/cm^2 for methanol and isopropanol, respectively. No significant response due to mass uptake was seen for iso-octane (kinetic diameter = 0.62 nm). These results serve as proof-of-principal that dramatic discrimination based on size exclusion effects can be obtained using controlled microstructure coatings.

Hydrous Oxide Ion Exchange Coatings

It is well known that hydrous oxides, such as sodium titanates or niobates, act as ion exchange materials with large ion exchange capacities. This capability can be used to advantage in nuclear waste applications [17] or in the preparation of catalysts which, due to the highly dispersed nature of the ion exchanged metal atoms, show high activity even at low metal loading [18]. By preparing coatings from these materials on acoustic plate mode (APM) devices, these large ion exchange capacities should result in large sensor responses during the exchange of ions from solution. Chemical selectivity can be varied by the choice of cations used (e.g., niobates form strongly acidic supports, titanates form amphoteric supports, and lanthanides form basic supports) and by controlling pore sizes.

To investigate the utility of these coatings, a sodium titanate system with a sodium:titanium ratio of 1:2 was chosen [17,18]. The standard preparation technique for this material results in a solution which thickens too quickly to be usable in forming homogeneous coatings. However, by diluting to 25% by volume in hexane, reasonably homogeneous coatings are formed by spin-coating at 4000 rpm. Film thickness per coat is 300 nm. Initial experiments investigated the APM response during the uptake of aqueous Ni^{2+} at pH 6. The APM response indicates the ion exchange is far from complete and is only partially reversible (significant amounts of exchanged Ni^{2+} appear to remain in the film after treatment with pH 3.0 HNO_3 and 1.0 M $NaNO_3$ solutions). This incomplete exchange contrasts results obtained for bulk samples with similar Ni^{2+} treatments [18].

To verify the APM results, similar coatings were formed on silicon and analyzed using a Tracor 5000 energy dispersive X-ray fluorescence (XRF) spectrometer. Based on the amount of titanium in the film, Ni^{2+} exchange is incomplete (only 6% after 10 min in a 0.05 M $Ni(NO_3)_2$ solution at pH 5.8). This incomplete exchange is verified by the observation that only 35% of the Na^+ initially present in the film was removed. The partial irreversibility of the Ni^{2+} exchange is consistent with the lack of an experimentally significant change in the Ni/Ti ratio after a pH 3.0 HNO_3 rinse, a subsequent 1.0 M $NaNO_3$ rinse and a subsequent 0.1 M EDTA (ethylenediaminetetraacetic acid) rinse at pH 6.5.

In contrast, XRF analysis of a second film for the ion exchange of Ag^+ indicates that exchange from a 0.05 M solution at pH 8 is effectively complete (97% of theoretical with only 3% of the initial Na^+ remaining in the film). In addition, the Ag^+ can be effectively removed from the film: only 23% remained after a pH 3.0 HNO_3 rinse, 15% after a subsequent 1.0 M

$NaNO_3$ rinse and 9% after a subsequent 0.1 M EDTA rinse. Based on these results, Ag^+ exchange experiments were performed on a second coated APM device. Peristaltic pumps were used to pump solutions to and from a cell holding the liquid in contact with the unelectroded side of the APM device.

The results, shown in Fig. 4, are in good qualitative agreement with the XRF data. When a pH 8.0 solution of NaOH is replaced with a 0.05 M $AgNO_3$ solution at the same pH, a frequency decrease of about 190 ppm is observed after an initial frequency increase. Assuming the frequency response is due to changes in the mass loading of the film, this shift corresponds to a change in the film mass density of 4.4 $\mu g/cm^2$. This value is significantly lower than the value of 70 $\mu g/cm^2$ calculated for complete exchange of Ag^+ for Na^+ based on the film thickness of 600 nm (two coats were used), a sodium titanate skeletal density of 2.4 g/cm^3, 40% porosity and a mass per ion exchange site of 177 g/mole (assumes site has form $HTi_2O_5^-$). This difference may indicate that many of the ion exchange sites are inaccessible. Work is ongoing with this system to determine the cause of this reduced response and to determine if the film-forming process can be altered to prepare coated APM devices which exhibit the dramatically larger response that is expected (full exchange of Ag^+ should give a frequency decrease of about 3000 ppm). The initial upward spike appears to be due to the loss of liquid flow which occurs during the change of solutions and was observed every time the solutions were changed. It should be possible to remove this spurious signal using a solvent delivery system that can change solutions without loss of flow.

When the pH 8.0 $AgNO_3$ solution is replaced with a NaOH solution at the same pH, a 60 ppm frequency increase is observed, indicating that about 30% of the Ag^+ is removed from the film. When a pH 3.0 HNO_3 solution is used, an additional frequency increase of over 110 ppm is observed. The total frequency increase in these two steps indicates that 90%

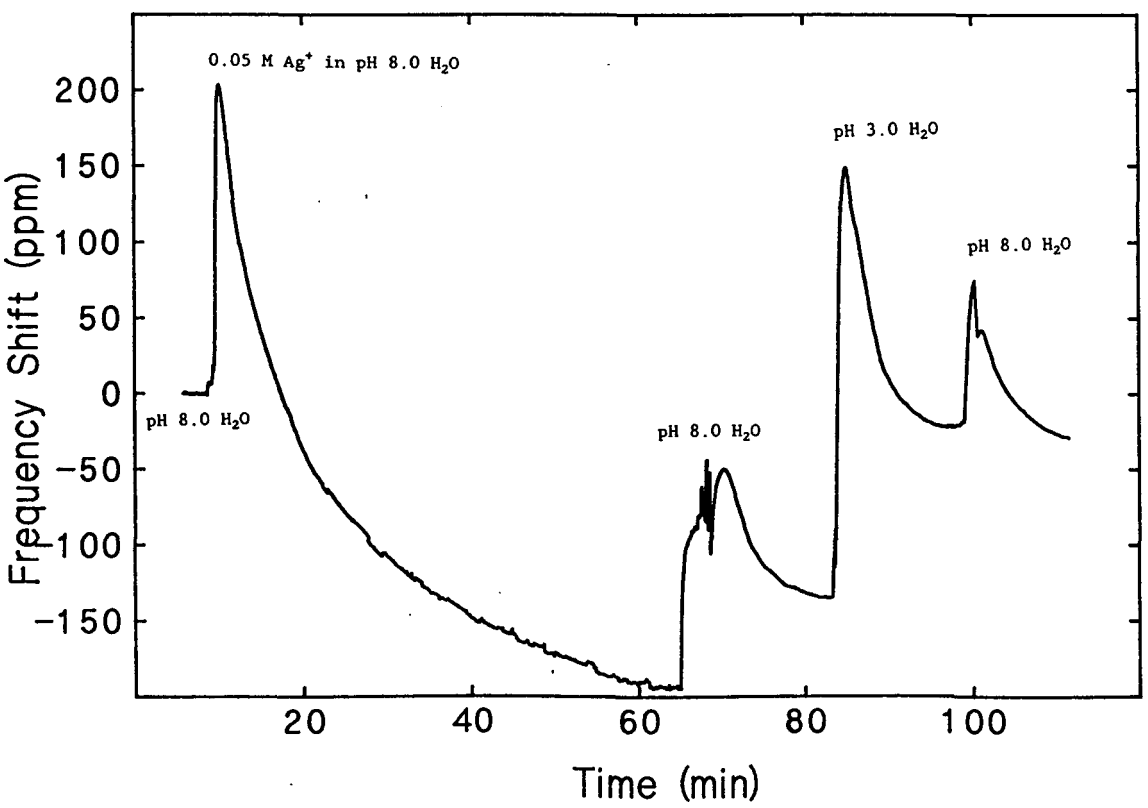

Fig. 4: Frequency response of sodium titanate-coated APM device during ion exchange of Ag^+. A mass increase of 4.4 $\mu g/cm^2$ is detected for this exchange. Reversibility is indicated by the frequency returning to near its original value after a pH 3.0 rinse.

of the exchanged Ag^+ has been removed, verifying the reversibility of this exchange process (this value may be a slight overestimate since the ion exchange sites will contain H^+ at this pH rather than Na^+ after the Ag^+ is removed). Except for the upward spike, a relatively small frequency shift is observed when the pH 3.0 HNO_3 solution is replaced with the pH 8.0 NaOH, indicating that the frequency increase seen with the pH 3.0 solution is due to mass loss during Ag^+ removal rather than due to some other effect related to the pH change. These results demonstrate that the large ion exchange capacities of hydrous oxide materials can be used to provide large sensor responses. Future work with these coatings will focus on: (1) optimizing the film-forming process to maximize sensor response and reproducibility, (2) determining the selectivity of the ion exchange process to ionic species of interest, and (3) investigating the variability in ion exchange properties obtainable with various hydrous oxides.

Surface Modification Using Silane Coupling Agents

Another technique being investigated to take advantage of the high surface area and controlled pore structure of sol-gel coatings is the derivatization of the coating surfaces with ligands that selectively bind chemical species of interest. The derivatizing agents used in this study are silane coupling agents (e.g., $XSi(OR)_3$ where R is an alkyl group and X is a ligand). The specific agent used, designated TMS-DETA, has a diethylenetriamine (DETA) ligand separated from the Si by a propyl chain: $(CH_3)_3Si(CH_2)_3NH(CH_2)_2NH(CH_2)_2NH_2$. Two techniques for performing this derivatization have been investigated.

The first technique involves the addition of the TMS-DETA to the sol-gel solution during preparation to form particles coated with DETA. Derivatized films could then be formed by dip- or spin-coating from this solution. This procedure was used to alter a sol-gel process to make particles with diameters of approximately 25 nm (based on the Stöber process [13]). The results are summarized in Table II. The TMS-DETA has a significant effect on the stability of the sol-gel solution: as the TMS-DETA concentration is increased, the system goes from a stable sol to flocculation to gelation. The uptake of Cu^{2+} after treatment with 1.0 M $Cu(NO_3)_2$, determined by dissolution of the sample and analysis by atomic absorption spectroscopy, appears to be stoichiometric with the amount of DETA used in the sol-gel preparation (i.e., one Cu^{2+} per DETA molecule). This indicates the ligands are accessible for binding from solution. In addition, a deep blue color is observed in the samples at higher DETA concentrations, typical of copper amine complexes. It was observed that this color lightened upon removal of water (sample is stored in a dry environment) and deepened upon exposure to water vapor. This is probably due to removal of water molecules which are acting to fill the fourth coordination site of the copper. If the dry sample is exposed to ammonia, the color deepens rapidly and remains dark even if placed in a dry environment, indicating that the ammonia molecule is more strongly attached due to its better ability to complex the copper. This sensitivity to ammonia could be used to prepare a dosimetric ammonia sensor from these coatings.

The second technique involves the preparation of a porous coating from a standard sol-gel solution followed by treatment of the surfaces of the sample with the TMS-DETA (from a dilute solution in ethanol). This technique allows the desired pore structure (allowing for the decrease in the pore dimensions due to the attached surface layer) to first be formed using already characterized sol-gel protocols. For this study, particulate silicate films were deposited by spin-coating a solution containing 29 nm diameter Stöber particles. XRF analysis indicated that the uptake of Cu^{2+} in the as-deposited film was less than 0.1 $\mu g/cm^2$ of film after a 5 minute treatment in 1 M $Cu(NO_3)_2$ followed by rinsing with deionized water. However, after the diethylenetriamine ligands were silane-coupled to the surfaces, the Cu^{2+} uptake from a similar treatment increased to 3.0 $\mu g/cm^2$. Based on the film thickness (800 nm) and the particle diameter, this amount of Cu^{2+} can be used to calculate the surface area

Table II: Gel behavior and uptake of Cu^{2+} for a sol-gel system prepared using the Stöber process altered by the addition of TMS-DETA.

Mole Percent		Gel		Color After
DETA/Si	Cu^{2+}/Si	Behavior	Appearance	Cu^{2+}
0.0	0.4	stable	granules	pale green
0.3	0.5	flocs	flakes	lt. blue
1.0	1.0	gels	chunks	deep blue
5.0	5.7	gels	chunks	v. deep blue

per DETA molecule (assuming the Cu^{2+} is bound stoichiometrically and that the film is 60% dense). The value calculated is 0.35 nm^2 per molecule, which represents about one DETA for every three Si at the surface. Since the silane coupling agent is trifunctional and can form three siloxane linkages, this value is in good agreement with a full coating of the DETA 3ligands on the surfaces of the film. This type of film is currently under test with APM devices. Since a wide variety of ligands with silane coupling groups are commercially available, this generic technique should be able to provide high surface area coatings with tailored chemical selectivities.

CONCLUSIONS

Sol-gel chemistry can be used to prepare thin oxide sensor coatings that provide both high sensitivity, due to high surface areas, and chemical selectivity, based on both steric and chemical factors. Coating microstructure can be evaluated by monitoring nitrogen adsorption/desorption at 77 K using SAW devices as sensitive microbalances. Gas and liquid phase AW sensor coatings based on zeolite/sol-gel, hydrous oxide ion exchange and surface-derivatized sol-gel coatings have been demonstrated.

The authors gratefully acknowledge helpful discussions and technical assistance of C. S. Ashley, S. L. Martinez, B. J. Lammie and K. L. Higgins (XRF) of Sandia National Laboratories and T. Bein and K. Brown (zeolite synthesis) of the University of New Mexico. This work was partially supported by the Energy Conversion and Utilization Program of the U. S. Department of Energy and was performed at Sandia National Laboratories, supported by the U.S. Department of Energy under contract number DE-AC04-76DP00789.

REFERENCES

1. C. J. Brinker and G. W. Scherer, Sol-Gel Science: The Physics and Chemistry of Sol-Gel Processing (Academic, San Diego, 1990).
2. C. J. Brinker, J. Non-Cryst. Solids, 100, 31 (1988).
3. C. J. Brinker, A. J. Hurd and K. J. Ward in Ultrastructure Processing of Advanced Ceramics, edited by J. D. Mackenzie and D. R. Ulrich (Wiley, New York, 1988), p. 223.
4. C. J. Brinker, G. C. Frye, A. J. Hurd, K. J. Ward and C. S. Ashley, in Proc. IVth Int. Conf. on Ultrastructure Processing of Glasses, Ceramics and Composites, edited by D. R. Uhlmann and D. R. Ulrich (Wiley, New York, 1990), in press.
5. M. S. Nieuwenhuizen and A. Venema, Sensors and Materials, 1, 261 (1989).

6. H. Wohltjen, Anal. Chem., 56, 87A (1984).
7. S. L. Rose-Pehrsson, J. W. Grate, D. S. Ballantine, Jr. and P. C. Jurs, Anal. Chem., 60, 2801 (1988).
8. B. J. Costello, B. A. Martin and R. M. White, in Proc. 1989 IEEE Ultrasonics Symp. (IEEE, New York, 1989), pp. 977-981.
9. S. J. Martin, A. J. Ricco, T. M. Niemczyk and G. C. Frye, Sensors and Actuators, 20, 253 (1989).
10. S. J. Gregg and K. S. W. Sing, Adsorption, Surface Area and Porosity, 2nd ed. (Academic, New York, 1982).
11. G. C. Frye, S. J. Martin, A. J. Ricco and C. J. Brinker, in Chemical Sensors and Microinstrumentation, edited by R. W. Murray, R. E. Dessy, W. R. Heineman, J. Janata and W. R. Seitz (ACS, Washington, 1989), Ch. 14.
12. C. L. Glaves, G. C. Frye, D. M. Smith, C. J. Brinker, A. Datye, A. J. Ricco and S. J. Martin, Langmuir, 5, 459 (1989).
13. W. Stöber, A. Fink and E. Bohn, J. Coll. Int. Sci., 26, 62 (1968).
14. T. Bein, K. Brown, C. J. Brinker, Studies in Surface Science and Catalysis, 49, 887 (1989).
15. G. C. Frye, A. J. Ricco, S. J. Martin and C. J. Brinker, in Better Ceramics Through Chemistry III, edited by C. J. Brinker, D. E. Clark and D. R. Ulrich (Mater. Res. Soc. Proc., 121, Pittsburgh, PA 1988), pp. 349-354.
16. T. Bein, K. Brown, G. C. Frye and C. J. Brinker, J. Amer. Chem. Soc., 111, 7640 (1989).
17. R. G. Dosch, T. J. Headley and P. Hlave, J. Amer. Cer. Soc., 67, 354 (1984).
18. B. C. Bunker, C. H. F. Peden, S. L. Martinez, E. J. Braunschweig and A. K. Datye, in Characterization and Catalyst Development: An Interactive Approach, edited by S. A. Bradley, M. J. Gattuso and R. J. Bertolacini (Amer. Chem. Soc., Washington, 1989), Ch. 8.